THE JOURNAL OF PHYSICAL CHEMISTRY B

pubs.acs.org/JPCB Article

Extracting the Frequency-Dependent Dynamic Stokes Shift from Two-Dimensional Electronic Spectra with Prominent Vibrational Coherences

Jiawei Lu, Yumin Lee, and Jessica M. Anna*

Cite This: J. Phys. Chem. B 2020, 124, 8857−8867 Read Online

ACCESS | Metrics & More | Article Recommendations | Supporting Information

ABSTRACT: The dynamic Stokes shift is a common means for characterizing ultrafast solvation dynamics of electronically excited states. Here we extract the excitation frequency-dependent dynamic Stokes shift from two-dimensional electronic spectra (2DES) of cresyl violet, a molecule with a well-defined vibronic progression. The extracted dynamic Stokes shift function, $S(t)$, exhibits oscillatory behavior, and the oscillatory components are assigned to intramolecular vibrational modes through DFT and TD-DFT calculations. The well-characterized oscillations are incorporated into the fitting procedure of $S(t)$. The excitation frequency dependence of the ultrafast response is examined through the analysis of $S(t)$ obtained from slices taken at different excitation frequencies of the 2DES spectra. The extracted ultrafast timescales range from 36 to 98 fs, and we interpret the frequency dependence of the timescales in the context of other dynamic processes that also lead to lineshape changes in the 2DES spectrum, such as vibrational energy relaxation and spectral diffusion. Through comparison of the extracted timescales, we find that the fastest timescales are extracted over a range of excitation frequencies, where contributions from vibrational relaxation and spectral diffusion can be minimized.

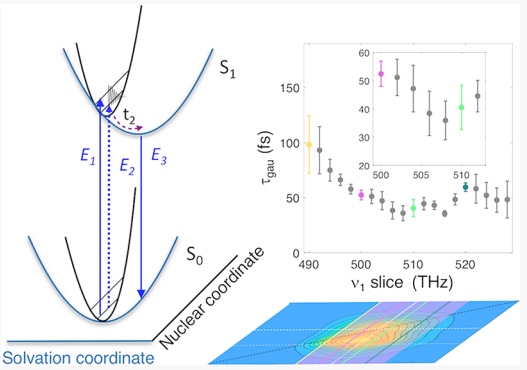

INTRODUCTION

Understanding the ultrafast dynamics that follow an electronic excitation is important for predicting the fate of an electronic excited state.[1−3] Prior to the absorption of a photon, a solute molecule lies in the ground electronic state and the surrounding solvent molecules can be considered at equilibrium with respect to the charge distribution associated with the molecule. Excitation of the solute to the Franck−Condon (FC) excited state induces a change in this charge distribution. As time evolves, the excited state begins to relax through intramolecular and intermolecular vibrational relaxation and solvent reorganization.[1,2,4−6] A schematic of this process is depicted in Figure 1 where FC active modes will evolve on the excited electronic state as vibrational energy is dissipated on the femtosecond to picosecond timescales. In addition, the solvent molecules lying in close proximity to the solute will respond to the charge rearrangement that accompanies the electronic excitation. For polar solvent molecules, the solvation dynamics can be classified into two contributions, an ultrafast sub-100 fs inertial response followed by a diffusive contribution that evolves on slower timescales.[1,7−12] The ultrafast response of the solvent can dictate the reactivity of the system,[2,3,6,13,14] for example, through stabilization of charge transfer states.[15−18] In addition, vibrational motion and relaxation can also play an important role in electron and proton transfer processes.[3,19−23] In this sense, understanding the ultrafast dynamics associated with the creation of an electronic excited state could lead to additional insight into the chemical reactivity of a system.

Two-dimensional electronic spectroscopy (2DES) is a powerful experimental technique for characterizing the ultrafast dynamics of electronic excited states.[24−30] One reason for this lies in the ability of 2DES to simultaneously probe ultrafast dynamics associated with different processes while maintaining high spectral and temporal resolution. For example, in the context of Figure 1, 2DES can probe the evolution of vibrational modes and ultrafast relaxation associated with the S_1 state.[30−32] In a 2DES experiment, the system is excited with ultrafast laser pulses leading to the creation of vibrational coherences on the ground and excited electronic states.[33−36] As the system relaxes the vibrational modes will evolve leading to amplitude modulations in the 2DES spectra, and analysis of the amplitude modulations yields information on the frequency and dephasing time of vibrational modes strongly coupled to the electronic excitation.[37−44] In addition to vibrational motion, 2DES is sensitive to the relaxation of the S_1 excited

Received: June 17, 2020
Revised: September 4, 2020
Published: September 9, 2020

https://dx.doi.org/10.1021/acs.jpcb.0c05522
J. Phys. Chem. B 2020, 124, 8857−8867

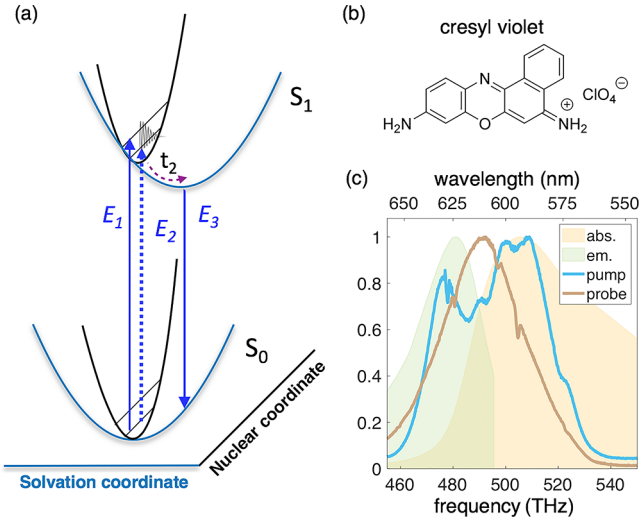

Figure 1. (a) Schematic depicting relaxation along the excited state potential energy surface. The three field-matter interactions in the 2DES experiment are indicated as blue lines. In this picture, a vibrational coherence is created in the excited electronic state during the t_2 time (where the solid/dotted arrow indicates interaction on the bra/ket side of the density matrix, respectively). (b) Chemical structure of cresyl violet perchlorate. (c) Linear absorption spectrum (orange shaded area) and fluorescence spectrum (green shaded area) of cresyl violet dissolved in methanol along with the spectra of the incoming pump (blue line) and probe (brown line) pulses.

state.[30−32,38,45−47] For 2DES performed on molecules with a larger Stokes shift, where the incoming laser pulses have been tuned to probe both the absorption and emission, relaxation of the excited electronic state manifests as a shift in frequency along the detection axis of the 2DES spectrum as the energy gap between the ground and excited state decreases.[29,47−51] This relaxation is referred to as the dynamic Stokes shift and can be described by the Stokes shift function,[4−6] $S(t)$ (eq 1), where $\nu(t)$ is the time-dependent frequency change associated with the energy gap between the ground state and excited electronic state, $\nu(0)$ is the initial transition frequency upon excitation, and $\nu(\infty)$ is the transition frequency associated with the relaxed system:

$$S(t) = \frac{\nu(t) - \nu(\infty)}{\nu(0) - \nu(\infty)} \tag{1}$$

Through the framework of linear response, $S(t)$ is equivalent to the frequency fluctuation correlation function (FFCF), normalized by the variance (eq 2):[4−6,15]

$$S(t) \cong M(t) = \frac{<\delta\omega_{eg}(t)\delta\omega_{eg}(0)>}{<\delta\omega_{eg}{}^2>} \tag{2}$$

It is through its relationship to the FFCF that the dynamic Stokes shift reports on the solvation dynamics of the system.[52]

There are several methods for extracting solvation dynamics from 2DES spectra,[40,53−57] including monitoring the dynamic Stokes shift.[47−50,58] Though extraction of the Stokes shift function can only be applied to systems where the evolution of the stimulated emission can be probed (systems with larger Stokes shifts), one advantage of this technique compared to other methods is that the dynamic Stokes shift function can be obtained from a single slice taken at a given excitation frequency in the 2DES spectrum.[48,50] In this sense, analysis of the dynamic Stokes shift can be used to resolve the frequency dependence of the solvation dynamics. However, as discussed above, there are additional contributions to the time evolution of the 2DES spectra, including the amplitude modulations that arise from the creation of vibrational coherences, and it is important to account for these processes in interpreting the extracted $S(t)$ functions. This is the focus of the current manuscript where we extract and analyze the frequency-dependent dynamic Stokes shift function from 2DES spectra containing prominent amplitude modulations arising from vibrational coherences.

As a model system, we investigate cresyl violet as it has a well-defined vibronic structure that has been previously characterized by 2DES,[59−64] pump−probe,[65−68] and Raman spectroscopies.[69,70] We present 2D electronic spectra of cresyl violet dissolved in methanol where the incoming pulses have been tuned to probe contributions from both the ground state bleach and stimulated emission. The 2DES spectra exhibit oscillatory behavior as expected based on the previous studies,[59−62] and the oscillations are assigned to vibrational coherences on the ground and excited electronic states through DFT and TD-DFT calculations. The time dependence of the well-characterized vibrational modes is then incorporated into the procedure for the analysis of the dynamic Stokes shift function, $S(t)$. The analysis is applied to $S(t)$ functions extracted from slices taken along the excitation axis (ν_1) and ultrafast timescales are obtained. We find that the ultrafast timescales vary between 36 and 98 fs across the excitation axis, and a comparison of the extracted timescales could serve as a means to disentangle vibrational relaxation from the inertial solvent response.

EXPERIMENTAL AND CALCULATION METHODS

Sample Preparation. Cresyl violet perchlorate (CAS number 41830-80-2) was purchased from Acros Organics and used without further purification. UV/VIS and 2DES measurements were performed on cresyl violet samples dissolved in methanol with an OD of ∼0.3 or less in a quartz cuvette with a pathlength of 1 mm (STARNA, 21-Q-1). UV/VIS spectra were measured on a JASCO V-750 spectrometer before and after the 2DES measurements to confirm the stability of the sample. Fluorescence spectra were measured on a HORIBA FL1039/40 fluorimeter in a quartz cuvette with a pathlength of 1.5 mm (STARNA, 16.12F-Q-1.5). All spectroscopic measurements were performed at room temperature using methanol as the solvent.

2DES. 2DES is a third-order nonlinear spectroscopy where a system undergoes three field-matter interactions (E_1, E_2, and E_3 (Figure 1)) that act to create a third-order polarization that leads to the emission of a signal (E_s).[71−74] The interaction with the first electric field, E_1, initiates the t_1 time period and creates a coherence between the ground and first excited electronic state of the system. The interaction with the second electric field, E_2, marks the end of the t_1 time period and the beginning of the t_2 time period. For the system of interest, cresyl violet, the second field-matter interaction can create either a population or a vibrational coherence on the ground or excited electronic state. The system is free to evolve in this state over the course of the t_2 time period. The interaction with the third electric field, E_3, acts to end the t_2 time period by creating another coherence between the ground and excited electronic state of the system. The interaction of E_3 marks the beginning of the t_3 time period, and the signal, E_s, is emitted.

https://dx.doi.org/10.1021/acs.jpcb.0c05522
J. Phys. Chem. B 2020, 124, 8857−8867

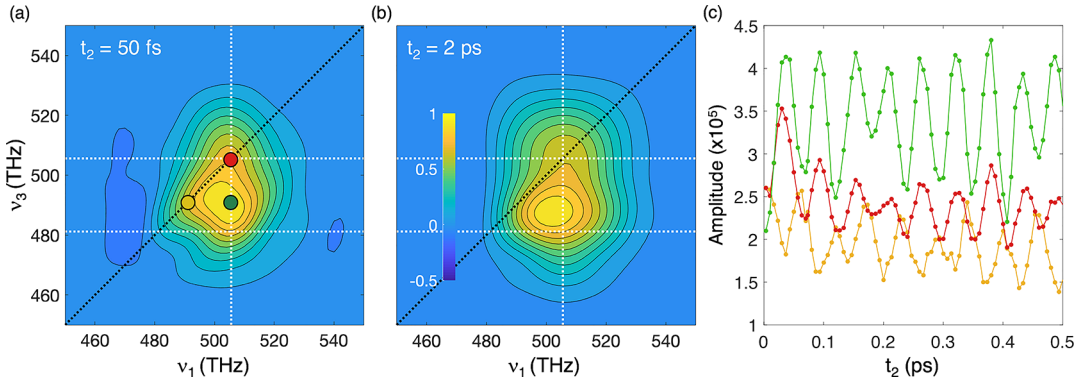

Figure 2. (a, b) Absorptive 2DES spectra of cresyl violet dissolved in methanol for two representative waiting times t_2 = 50 fs and t_2 = 2 ps. The dotted line along the ν_1 axis indicates the maximum of the absorption spectrum (505 THz), and the two dotted lines along the ν_3 axis indicate the maximum in the absorption (505 THz) and emission (481 THz) spectra. (c) Waiting time-dependent amplitudes at three different ν_1,ν_3 coordinates: ν_1,ν_3 = 490, 490 THz (yellow), ν_1,ν_3 = 505, 505 THz (red), and ν_1,ν_3 = 505, 490 THz (green), are plotted. The ν_1,ν_3 coordinates are denoted as colored dots superposed on the 2DES spectrum at t_2 = 50 fs.

Experimentally, for each t_2 time period, the t_1 time period is scanned and the resulting signal is detected through spectral interferometry. A Fourier transform along the t_1 axis yields the excitation axis, ν_1. The detection axis, ν_3, is obtained experimentally by the diffraction grating in the spectrometer. The resulting 2D spectrum can be considered a correlation map between the excitation frequencies and the detection frequencies.[24,30]

Our 2DES experimental setup has been described in detail previously.[50,75] Briefly, 2DES spectra were obtained in the pump−probe geometry using a pulse shaper-based design[51,76,77] ensuring that purely absorptive 2D spectra are collected directly.[51,76−78] An acousto-optic programmable dispersive filter pulse shaper (DAZZLER, FASTLITE) was used to scan the t_1 time delay from −50 to 0.1 fs in 0.2 fs step sizes. For each t_1 time delay, a four pulse phase-cycling scheme was applied to remove the background and scattering,[76] and for a given phase relationship, 50 spectra were averaged. The measurements were performed using the partially rotating frame with a frame rotation frequency of 350 THz.[76] The t_2 time was scanned from −20 fs to 2.2 ps in 7 fs step sizes using a computer-controlled delay stage (NEWPORT ILS250 CC, XPS-Q8). The incoming pulses were tuned to overlap with the absorption and fluorescence spectra, and the spectra of the incoming pulses are plotted in Figure 1. The pulses were characterized by SFG-FROG,[79] which showed a temporal duration of ∼21 fs at the FWHM for the cross correlation between the pump and probe pulses (Figure S1 in the Supporting Information). The two pump pulses had a total power of 10 nJ at the sample (5 nJ per pulse) and the probe pulse had a power of 5 nJ. The pulses were set to the magic angle polarization: horizontal for the probe pulse, and 54.7° for the pump pulse with respect to the polarization of the probe pulse.

Calculations. DFT and TD-DFT calculations were performed with the Gaussian16 software package.[80] Ground state and excited state geometry optimizations were performed at the B3LYP level of the theory with the 6-311+G(2d,p) basis set, which was used for similar laser dyes.[50,81] For all calculations, the polarizable continuum model (PCM) was used to account for the dielectric of the methanol solvent. Frequency calculations were performed to confirm that the optimized geometries were at a minimum on the potential energy surface. The non-resonant Raman active vibrational modes were calculated using the optimized geometry of the S_0 state. The dipole strengths associated with the Franck−Condon absorption and emission transitions were calculated from the optimized geometries for the S_0 and S_1 states. The optimized Cartesian coordinates for the S_0 and S_1 states, the calculated vibrational spectra, and additional calculation details are reported in the Supporting Information.

RESULTS AND DISCUSSION

2DES Spectra of Cresyl Violet. Absorptive 2DES spectra of cresyl violet in methanol are shown in Figure 2 for two representative waiting times t_2 = 50 fs and t_2 = 2 ps. The maximum of the linear absorption spectrum ($\nu_{max,abs}$ = 505 THz) and fluorescence spectrum ($\nu_{max,fl}$ = 481 THz) are indicated on the 2DES spectra as white dotted lines. The 2D spectral profile is filtered by the incoming laser pulses, which were tuned to spectrally overlap with both the linear absorption and fluorescence spectra. The spectra of the incoming pump and probe pulses are plotted in Figure 1. This tuning gives a spectral window by which to observe the time evolution associated with both the ground state bleach and the stimulated emission.

As the waiting time increases the main peak undergoes an asymmetric line broadening along the ν_3 axis, with the maximum amplitude shifting toward $\nu_{max,fl}$ as t_2 increases. Many previous 2DES studies have attributed this red shift to the dynamic Stokes shift.[46−51] After the initial electronic excitation, the excited system starts to relax in response to the altered charge distribution of the S_1 excited state through solvent reorganization and/or intramolecular vibrational energy relaxation. As the S_1 state relaxes, the energy gap between the ground state and the excited state decreases, leading to a red shift in the stimulated emission. In the 2DES spectra, this red shift leads to a shift in the amplitude of the peak to lower frequencies along the ν_3 axis. We extract the dynamic Stokes shift function from the 2DES spectra by monitoring this peak shift as a function of time.

In addition to lineshape changes, we also observe amplitude modulations that arise from the creation of vibrational coherences on the ground and excited electronic states.[28,37−44] Time-dependent amplitude traces are plotted in Figure 2 for three different ν_1,ν_3 coordinates: ν_1,ν_3 = 490, 490 THz (yellow), ν_1,ν_3 = 505, 490 THz (green), and ν_1,ν_3 = 505, 505 THz (red). As the waiting time evolves the amplitude

https://dx.doi.org/10.1021/acs.jpcb.0c05522
J. Phys. Chem. B 2020, 124, 8857−8867

oscillates, consistent with previous 2DES studies performed on cresyl violet. These previous studies focused on analyzing these oscillations: to assign vibrational coherences on the ground and excited electronic states,[59] to expand experimental techniques,[60−63] and to report on photophysical and photochemical events.[64] In this manuscript, we consider how to incorporate these prominent amplitude modulations into the analysis of the dynamic Stokes shift.

To account for the oscillatory components in the dynamic Stokes shift function, we first extract the frequencies of the vibrational coherences from the 2DES spectra and characterize the coherences through comparison with DFT and TD-DFT calculations.

Vibrational Coherences. To extract the frequencies of the vibrational coherences, we fit the t_2-dependent amplitudes at each ν_1,ν_3 coordinate with a biexponential function to remove the background associated with population dynamics. The resulting residuals are then Fourier transformed along the t_2 axis to yield the power spectra. The power spectra obtained from analysis of the traces at the three different ν_1,ν_3 coordinates (see colored dots in Figure 2a) are shown in Figure 3a using the same color-coding scheme as Figure 2. Comparison of the traces shows that the amplitude of the oscillatory components varies for different ν_1,ν_3 coordinates in the 2D spectra. As we are interested in extracting all the oscillatory components present in the 2D spectra, we focus on the averaged power spectrum obtained from taking the mean of the power spectra at each ν_1,ν_3 coordinate within a box spanning ν_1 = 450−550 THz and ν_3 = 450−550 THz in the 2D spectrum. The averaged power spectrum is displayed in Figure 3b as a blue line. Given our experimental conditions, the spectral overlap of the incoming pump pulse coupled with the temporal bandwidth of ∼21 fs, we resolve six oscillatory features with frequencies of 343, 470, 520, 567, 587, and 666 cm^{-1}. The frequencies are consistent with previous ultrafast spectroscopic studies[62,65−68] and Raman studies[69,70] on cresyl violet. The experimentally determined frequencies are indicated as blue vertical dotted lines in Figure 3 and are reported in Table 1.

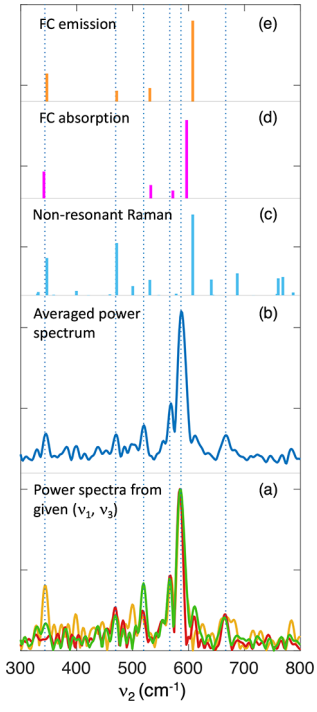

Figure 3. (a) Power spectra associated with the t_2 traces at ν_1,ν_3 = 490, 490 THz (yellow), ν_1,ν_3 = 505, 505 THz (red), and ν_1,ν_3 = 505, 490 THz (green), the three coordinates in Figure 2a. (b) Average power spectrum for the ν_1,ν_3 coordinates in the 2DES spectra within the ν_1 = 450−550 THz and ν_3 = 450−550 THz range. The six light blue dotted lines indicate the most prominent modes in the averaged power spectrum. (c) Calculated non-resonant Raman spectrum. (d) Calculated dipole strength associated with the FC absorption. (e) Calculated dipole strength associated with the FC emission.

Table 1. Frequencies of the Oscillatory Components from the 2DES Spectra Are Reported Along with the Frequencies of the Assigned Vibrational Modes from DFT and TD-DFT Calculations

	calculated frequencies		
2DES power spectrum (cm^{-1})	Raman active modes (cm^{-1})	FC absorption (cm^{-1})	FC emission (cm^{-1})
343	347	342	347
470	472		472
520	531	533	531
567		572	
587	608	597	608
666	687		

To assign the observed frequencies to vibrational coherences, we compare the experimental results to those obtained from quantum chemical calculations. Due to the temporal short pulses used to obtain the 2DES spectra, vibrational coherences on both the ground and excited electronic states will be created.[33−36] To describe the vibrational coherences created on the excited electronic state, we calculated the FC active modes associated with absorption. The calculations show four FC active modes lying within the 300−800 cm^{-1} spectral region. The calculated frequencies are reported in Table 1, and the FC dipole strength is plotted as a function of frequency (pink stick spectra) in Figure 3. To describe the vibrational coherences created on the ground electronic state, we calculated the FC active modes associated with the emission spectrum and the non-Resonant Raman active modes. The FC emission calculation accounts for vibrational coherences created on the electronic ground state as the excited electronic state relaxes during the t_1 time period. The dipole strength associated with the FC emission is plotted as a function of frequency in Figure 3 (orange sticks), and the frequencies are reported in Table 1. In addition, we calculated the non-resonant Raman active modes to account for the vibrational modes excited through impulsive Raman processes. The calculated Raman spectrum is plotted in Figure 3 (cyan sticks) in the 300−800 cm^{-1} spectral region, and the assignment procedure is detailed in the Supporting Information.

Figure 3 allows for a comparison of the experimental frequencies with the calculated vibrational frequencies associated with the Raman active and FC active modes. Of the six experimentally resolved vibrational frequencies, three frequencies, 343, 520, and 587 cm^{-1}, appear in all three calculations, indicating that these oscillations could arise from vibrational coherences created on both the ground and excited electronic states. We note that previous pump−probe measurements performed on cresyl violet[65] were able to

https://dx.doi.org/10.1021/acs.jpcb.0c05522
J. Phys. Chem. B 2020, 124, 8857−8867

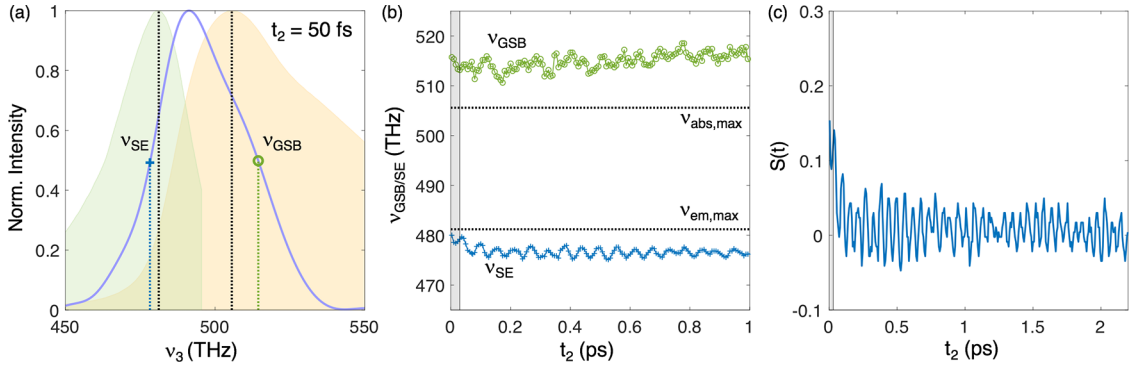

Figure 4. (a) Representative projection of the 2DES spectrum at t_2 = 50 fs (blue line) and the linear absorption spectrum (orange shaded area) and emission spectrum (green shaded area). The two black dotted lines indicate the maximum in the absorption (505 THz) and emission (481 THz) spectra. ν_{SE} (blue vertical line) and ν_{GSB} (green vertical line) at t_2 = 50 fs are plotted at the frequency closest to 50% of the maximum intensity of the projected 2DES spectrum. (b) Plots of ν_{SE} (blue plus sign line) and ν_{GSB} (green open circle line) as a function of waiting time t_2. The two black dotted lines indicate the maximum in the absorption (505 THz) and emission (481 THz) spectra. The gray area (up to 28 fs) indicates the time period of the coherent artifacts due to the pulse overlap and is not analyzed. (c) Stokes shift function $S(t)$ (eq 1) generated from analysis of the projections of the 2DES spectra onto the ν_3 axis.

resolve the contributions from the ground state and excited state coherences to the peak at 590 cm^{-1}. As our experimental resolution is limited by the maximum t_2 scanned, we do not separate this peak into contributions from the ground or excited state coherences but assume that both contributions could be present. Based on the calculations, we assign the experimental mode at 567 cm^{-1} to a vibrational coherence on the excited electronic state as it is only present in the Franck−Condon absorption calculation and absent in the ground state Raman and Franck−Condon emission calculations. This is consistent with previous spontaneous Raman measurements by Fujiyoshi *et al.* that studied the low frequency vibrations of cresyl violet where the 567 cm^{-1} mode was not observed in the spontaneous Raman measurement.[69] The 470 and 666 cm^{-1} modes are assigned to vibrational coherences on the ground electronic state as they are only present in the calculated Franck−Condon emission and/or non-resonant Raman spectra and absent in the FC absorption spectrum. Again, this assignment is consistent with a previous Raman study.[69]

Through comparison with the calculated spectra and previous studies, we have assigned the amplitude modulations in the 2D electronic spectra to vibrational coherences where the coherences can evolve on the ground and/or excited electronic state. We now incorporate these well-characterized coherences into the analysis of the dynamic Stokes shift.

Dynamic Stokes Shift. To extract the dynamic Stokes shift function from the 2DES spectra, we analyze the linewidth changes along the ν_3 axis according to our previously described procedure.[50] We first demonstrate the importance of including amplitude modulations in the analysis of the dynamic Stokes shift obtained from the projections of the 2DES spectra onto the ν_3 axis. We then apply this procedure to investigate the frequency dependence of the dynamic Stokes shift where the dynamic Stokes shift function is obtained from taking slices at different excitation frequencies (ν_1).

To obtain the projections, each 2DES spectrum is summed along the ν_1 axis for a given t_2 time. A representative projection for t_2 = 50 fs is plotted in Figure 4a as a blue line along with the linear absorption (orange area) and fluorescence (green area) spectra. Given the tuning of the incoming laser pulses, the stimulated emission and ground state bleach spectral features are not clearly resolved; however, a comparison with the absorption and fluorescence spectra indicates that the lower energy portion of the projection will have more contribution from the stimulated emission, and the higher energy portion will have more contribution from the ground state bleach. Using the lower energy portion as a reporter for the stimulated emission, we extract the transition frequency associated with the stimulated emission, ν_{SE}, recording the frequency where the amplitude reaches 50% of the maximum amplitude on the lower energy portion of the projection. For comparison, the frequency associated with the ground state bleach, ν_{GSB}, is extracted through taking the frequency where 50% of maximum amplitude is reached for the higher energy portion of the projection.

For the representative projection in Figure 4a, the extracted frequencies for ν_{SE} and ν_{GSB} are marked with vertical dotted lines. As mentioned above, ν_{SE} will have a larger contribution from the stimulated emission. As the stimulated emission reports on the evolution of the S_1 excited state, ν_{SE} serves as a reporter for the energy gap between the S_1 and S_0 state in the 2DES spectra and its time evolution is plotted in Figure 4b. The plot shows that ν_{SE} decays over the first 200 fs. In addition, strong oscillatory features are observed as amplitude modulations arising from the creation of vibrational coherences that also contribute to the time evolution of the 2D electronic spectra.

From the time dependence of ν_{SE}, we can obtain the dynamic Stokes shift (eq 1) where $\nu(t)$ is taken as $\nu_{SE}(t_2)$. The $\nu(\infty)$ term is obtained from the longer time behavior of $\nu_{SE}(t_2)$, and the denominator $(\nu(0) - \nu(\infty))$ is equivalent to the steady-state Stokes shift obtained from the difference between the maxima of the linear absorption and fluorescence spectra, 24 THz for cresyl violet in methanol. The $S(t)$ obtained from the projection is plotted in Figure 4c. Figure 4c shows that $S(t)$ oscillates and decays as a function of waiting time t_2.

The decay in $S(t)$ is attributed to the solvation dynamics. Previous studies have shown that the decay of $S(t)$ for chromophores dissolved in methanol and other polar solvents can be well described with a Gaussian and exponential function.[8,14,82−84] The Gaussian function accounts for the inertial solvent response and the exponential function accounts for the diffusive solvent response. In addition to the decay in

https://dx.doi.org/10.1021/acs.jpcb.0c05522
J. Phys. Chem. B 2020, 124, 8857−8867

$S(t)$, we also observe oscillatory behavior. The oscillations arise from intramolecular vibrational coherences of cresyl violet that give rise to amplitude modulations in the 2DES spectra (see above section) and are not attributed to the intermolecular modes associated with the solvent. This is consistent with previous photon echo experiments performed with ultrafast laser pulses, where oscillations in the extracted correlation functions were assigned to the high frequency intramolecular vibrational modes of the excited chromophore.[8,84−88] These previous studies employed a cosine function to mimic the intramolecular mode and extract the timescales for solvation. Here, we take a similar approach by incorporating the well-characterized vibrational coherences into the analysis of the $S(t)$ function extracted from the 2DES spectra. We note that this procedure can be expanded on to account for the damped oscillatory components through applying a global analysis by following procedures outlined in previous pump−probe studies.[89,90]

To incorporate the vibrational modes into $S(t)$, we first model the $S(t)$ function with a Gaussian and single exponential function. We then analyze the resulting residuals, $R_{S(t)}$, to determine the frequencies and confirm the assignment of the oscillatory behavior. This information is then incorporated into the fitting procedure of $S(t)$. Additional information regarding the fitting procedure and initial guess parameters is reported in section 3 of the Supporting Information.

For $S(t)$ extracted from the projection of the 2DES spectra, the best fit using a Gaussian and exponential function is plotted in Figure 5a. We note that, given the temporal duration of the incoming pulses, we do not analyze the data points obtained within the first 28 fs. As the longest t_2 time probed is 2.2 ps, we do not fully characterize the diffusive component and have set the decay of the exponential function to a constant of ∼1 ps based on previous literature values.[8,88,91] Given the maximum waiting time probed, we focus our attention on the inertial response. The best fit yields a sub-100 femtosecond component of 29 ± 3 fs for the Gaussian component, and this is attributed to the inertial response of methanol.

The residual, $R_{S(t)}$, resulting from subtracting the Gaussian and exponential fit from the $S(t)$ function is plotted in Figure 5b and shows strong oscillatory features. Figure 5c plots the Fourier transform of the residual. Four oscillatory features are observed having frequencies of 342 cm^{-1}, 523 cm^{-1}, 566 cm^{-1} and 589 cm^{-1}. We note that these frequencies match well with vibrational coherences from the calculations (Figure 3 and Table 1) further confirming the assignment of the oscillations to vibrational modes of the chromophore.

As $S(t)$ is obtained from monitoring the transition frequency associated with the stimulated emission (ν_{SE}), one may expect the oscillatory behavior of $S(t)$ extracted from the 2DES spectra to arise from vibrational coherences on the electronic excited state. We find that the oscillatory components observed do coincide with the four oscillatory features present in the FC absorption calculation. However, three of these modes may also arise from ground state coherences. The ground state vibrational coherences can contribute to the extracted $S(t)$ due to possible overlapping spectral features in the 2DES spectra. For example, according to the displaced oscillator model, for a given vibrational mode having a frequency of ν_{vib}, one would predict a six peak pattern associated with ground state bleaching features in the 2DES absorptive spectra.[43,92−94] The six peak pattern consists of two diagonal peaks and their corresponding crosspeaks, where the energy difference

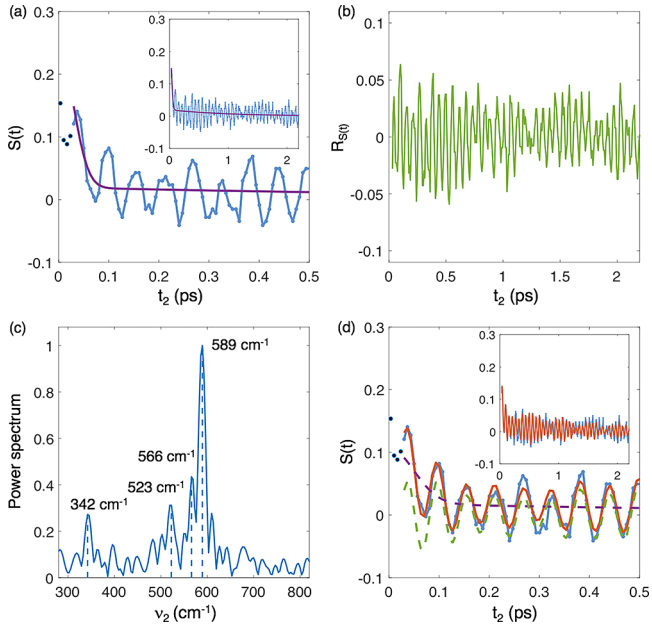

Figure 5. (a) Stokes shift function $S(t)$ (blue dots and line) from the projections of the 2DES spectra onto the ν_3 axis and the best fit from the sum of a Gaussian and single exponential decay function (magenta line). Inset plots $S(t)$ up to 2.2 ps and the main plot zooms in on the first 500 fs. (b) Residual, $R_{S(t)}$, obtained by subtracting the fit in (a) from $S(t)$. (c) Fourier transform of the residual ($R_{S(t)}$). The frequencies of the four prominent oscillatory components are marked with the blue vertical dashed lines. (d) Stokes shift function $S(t)$ (blue dots and line) from the projections of the 2DES spectra onto the ν_3 axis and the fit with the sum of a Gaussian and single exponential decay function along with four cosine functions (red line). The dashed lines indicate the different components of the fit with the magenta dashed line plotting the sum of a Gaussian and single exponential decay function and the green dashed line plotting the sum of the four cosine functions. The inset plots $S(t)$ up to 2.2 ps, and the main plot zooms in on the first 500 fs.

between the transitions corresponds to ν_{vib}. In addition, pathways that lead to the creation of populations in vibrational excited states of the ground electronic state will lead to two additional peaks that are shifted to lower frequencies along the ν_3 axis, with the frequency shift being equivalent to the frequency of the vibrational mode, ν_{vib}. If the frequency of the vibrational mode is comparable to the frequency shift associated with the Stokes shift, then these transitions may lead to oscillatory behavior in the region where ν_{SE} is extracted from the 2DES spectra. In this way, contributions from vibrational coherences in the ground electronic state could contribute to the oscillations in ν_{SE} and therefore $S(t)$.

To account for the influence that the vibrational coherences have on the extraction of the inertial solvent response, the periodic oscillations are included in the model to extract the solvent relaxation parameters. The four oscillatory modes are included in the model as damped cosine functions along with the Gaussian and single exponential functions. The extracted Gaussian timescale is reported in Table 2, and the resulting fit is plotted as a red solid line in Figure 5d. Parameters associated with the vibrational coherences are reported in Table S5 of the Supporting Information.

Accounting for the vibrational coherences, a timescale of 47 ± 4 fs for the inertial response is extracted from the analysis of the projection of the 2D electronic spectra onto the ν_3 axis. For

https://dx.doi.org/10.1021/acs.jpcb.0c05522
J. Phys. Chem. B 2020, 124, 8857−8867

Table 2. Best Fit Parameters for the Ultrafast Relaxation Timescales of Cresyl Violet in Methanol[a]

	A_{gau}	τ_{gau} (fs)	A_{exp}	τ_{exp} (ps)
$M(t)$ fitting parameters from the analysis of the projections of the 2DES spectra onto the ν_3 axis				
oscillatory modes not included in $M(t)$[b]	0.219 ± 0.045	29 ± 3	0.020 ± 0.005	1
oscillatory modes included in $M(t)$[c,d]	0.094 ± 0.011	47 ± 4	0.018 ± 0.002	1
$M(t)$[c,e] fitting parameters from the analysis of four representative slices taken at different ν_1 excitation frequencies				
slice at ν_1 = 490 THz	0.034 ± 0.009	98 ± 26	0.023 ± 0.003	1
slice at ν_1 = 500 THz	0.104 ± 0.010	52 ± 4	0.023 ± 0.002	1
slice at ν_1 = 510 THz	0.160 ± 0.038	40 ± 7	0.005 ± 0.006	1
slice at ν_1 = 520 THz	0.090 ± 0.019	60 ± 10	0.006 ± 0.005	1

[a]Error bars report 95% confidence intervals. $M(t)$ functions used are denoted with superscripts. The relaxation times and weights are estimated by the following expressions: [b]oscillatory modes are not included in $M(t)$: $M(t) = A_{gau}e^{-t^2/2\tau_{gau}^2} + A_{exp}e^{-t/\tau_{exp}}$; [c]oscillatory modes included in $M(t)$: $M(t) = A_{gau}e^{-t^2/2\tau_{gau}^2} + A_{exp}e^{-t/\tau_{exp}} + \sum_i^4 A_{vib,\,i}\cos(2\pi\nu_i t - \varphi_i)e^{-t/\tau_{vib,\,i}}$; [d]$A_{vib,\,i}$, ν_i, φ_i, and $\tau_{vib,\,i}$ for analysis of the projection are reported in Table S5 of the Supporting Information; and [e]$A_{vib,\,i}$, ν_i, φ_i, and $\tau_{vib,\,i}$ for analysis of the slices taken at different excitation frequencies are reported in Table S6 of the Supporting Information.

comparison, a timescale of 29 ± 3 fs was extracted when the oscillatory components were not accounted for. Comparing the two Gaussian and exponential fits, magenta lines in Figure 5a,d show that incorporating the oscillations ensures that the initial Gaussian component bisects the oscillations. Without incorporating the oscillations, the Gaussian component tends to only describe the first period of the oscillation. Based on the comparison, we show that for systems with strong vibrational coherences the inclusion of the damped oscillations in the fitting procedure is important for extraction of the inertial solvent response from the dynamic Stokes shift function obtained from 2DES spectra.

Frequency Dependence of the Dynamic Stokes Shift. We now apply the same procedure demonstrated with the projected 2D data to that of $S(t)$ obtained from slices taken at different ν_1 frequencies in the 2DES spectra. Here a slice at a given ν_1 frequency along the ν_3 axis can be thought of as narrow band pump−probe spectrum that maintains a high temporal resolution. In this sense, by taking slices at different ν_1 frequencies, it is possible to analyze the excitation-dependent behavior of the ultrafast solvation dynamics.

Slices were taken from the 2DES spectra at ν_1 frequencies ranging from 490 to 528 THz in 2 THz steps. For each slice, ν_{SE} is extracted and recorded for each waiting time using the same procedure described for the projection. The $S(t)$ functions for four representative slices taken at ν_1 equal to 490, 500, 510, and 520 THz are plotted in Figure 6. The ν_1 frequencies of the slices are indicated as colored lines on the 2DES spectrum (Figure 6a). The timescale associated with the Gaussian component is extracted using cosine functions to account for the oscillatory components along with a Gaussian and exponential function to describe the solvation dynamics. The extracted timescales for the Gaussian components, τ_{gau}, are reported in Table 2 (bottom), and the extracted fits are plotted in Figure 6b using the same color-coding scheme in Figure 6a for the four representative slices. The optimized parameters associated with the oscillations are reported in Table S6 of the Supporting Information. We note that, for most slices, within error, the frequencies of the oscillatory components are the same as those used for fitting the model to the $S(t)$ from the projection. However, for slices taken on the blue edge of the peak (the higher frequency edge), the 676 cm^{-1} mode is more prominent, and the 342 cm^{-1} mode shows less contribution, which is consistent with 2DES spectra interpreted through the displaced oscillator model.[43,92−94]

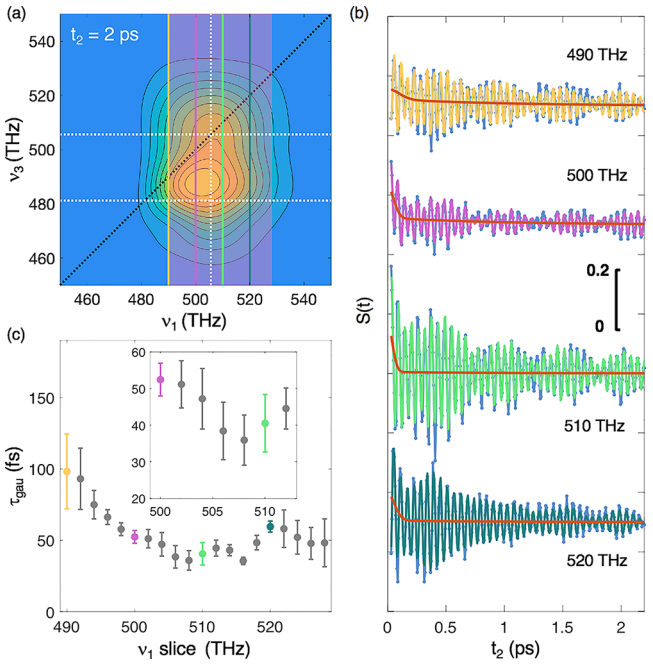

Figure 6. (a) The light red area superposed on the 2DES spectrum denotes the region where ν_1 slices were taken from the 2DES spectra. Four representative slices taken at ν_1 = 490 THz (yellow), 500 THz (magenta), 510 THz (light green), and 520 THz (dark green) are indicated as vertical lines. (b) The Stokes shift function $S(t)$ (blue) along with the corresponding fit (using the same color coding as in (a)) are plotted for the four representative slices. Here the red solid lines correspond to the Gaussian and single exponential component of the fit. (c) The extracted ultrafast timescales are plotted as a function of the ν_1 frequency of the slice. The inset zooms in on the 500−512 THz region where the fastest timescales are observed.

Comparison of the extracted τ_{gau} timescales in Table 2 shows that τ_{gau} varies as a function of the ν_1 excitation frequency, with slices taken near the center of the peak resulting in faster timescales. To further investigate this trend in frequency dependence, the extracted τ_{gau} are plotted as a function of the ν_1 slice frequency for each slice taken from the 2DES spectra in Figure 6c. The τ_{gau} associated with the representative slices are color coded using the same color scheme defined in Figure 6a. We find that the Gaussian components extracted from the center of the peak ∼508 THz have the fastest timescale of ∼36 ± 7 fs, while the Gaussian

https://dx.doi.org/10.1021/acs.jpcb.0c05522
J. Phys. Chem. B 2020, 124, 8857−8867

components associated with excitation to the red and blue of this frequency range have slower timescales ranging from ~50 to 100 fs. We note that additional 2DES data sets were obtained under different pulse tuning conditions to further test this analysis procedure and the ν_1 frequency dependence of the extracted timescales. The additional 2DES spectra and analysis are reported in section 4 of the Supporting Information. We find a similar behavior further supporting the analysis procedure.

To interpret the observed ν_1 frequency dependence of τ_{gau}, we consider how other dynamic processes contribute to the peak in the 2DES spectra. Both vibrational relaxation and spectral diffusion have a ν_1 frequency dependence and could lead to changes in the ν_3 linewidth. Here, we consider how these two processes will present in the analysis procedure for the extraction of the dynamic Stokes shift from the 2D spectra.

We first consider vibrational relaxation. When performing a 2DES experiment, the different vibrational states that lie within the bandwidth of the incoming laser pulses will be excited. As the system evolves, the excited vibrational states will relax, resulting in a growth below the diagonal, on the blue edge (higher frequency) of the peak along the ν_1 axis, in what would be the crosspeak region if it could be resolved. Taking a slice at higher lying ν_1 frequencies could be effectively selecting spectral changes more associated with this vibrational relaxation. In this sense, the process of vibrational relaxation could lead to a change in the amplitude profile and linewidth of the ν_1 slice, thus altering the frequency extracted for $\nu_{SE}(t_2)$ and contributing to the extracted Gaussian component.

In addition to vibrational relaxation, the peaks can also undergo spectral diffusion as the inhomogeneously broadened peak decays to a homogeneously broadened peak. In 2D spectra, this leads to a 2D lineshape change where the inhomogeneity is manifested as an elongation along the diagonal, and the decay in inhomogeneity results in a decay of this elongation.[71,72,74] This lineshape change is well known in 2D spectra, and its analysis serves as another means for extracting information regarding solvation dynamics from 2DIR and 2DES spectra.[40,53,54,95−97] Here we consider how the lineshape change associated with spectral diffusion could alter $\nu_{SE}(t_2)$ extracted from the ν_1 slices taken from the 2DES spectra. As a model, we first focus on a single transition where spectral diffusion can be described with a Kubo lineshape[72] (see Figure S15 in the Supporting Information for modeled spectra). As the Kubo lineshape does not account for the relaxation of the S_1 state, this model enables an examination of lineshape changes solely arising from spectral diffusion. To describe the lineshape changes associated with spectral diffusion, we interpret normalized spectra and slices through the parameter ν_{SD}, which is defined as the frequency where the amplitude reaches 50% of the maximum amplitude on the lower energy portion of the slice when only spectral diffusion is included in the model. We note that this is the same procedure used to extract $\nu_{SE}(t_2)$ when a Stokes shift is present, and in this sense the ν_1 excitation frequency dependence of ν_{SD} can be used to understand how spectral diffusion influences $\nu_{SE}(t_2)$. In considering spectral diffusion, slices taken at higher ν_1 frequencies (on the blue edge of the peak) will result in a decay of ν_{SD} to lower frequencies along the ν_3 axis. For ν_1 slices taken at lower ν_1 frequencies (on the red edge of the peak), spectral diffusion will result in an increase in ν_{SD} to higher frequencies along the ν_3 axis. For ν_1 slices taken at the center of the peak, spectral diffusion will also lead to a decay associated with ν_{SD} but to a lesser extent compared to slices taken on the blue edge of the peak. A comparison of ν_{SD} extracted from slices taken at different ν_1 frequencies of the simulated 2D spectra is made in Figure S15 of the Supporting Information. The described method for extracting $\nu_{SE}(t_2)$ from the ν_1 slices assumes that the lineshape changes along the ν_3 axis are dominated by the relaxation of stimulated emission. Given that spectral diffusion also results in lineshape changes along the ν_3 axis this process will contribute to the extracted $\nu_{SE}(t_2)$. Given the larger changes in ν_{SD} on the blue edge of the peak and the positive trend of ν_{SD} on the red edge of the peak, we expect the extraction of the $\nu_{SE}(t_2)$ from the ν_1 slices on the red and blue edges to have more contributions from lineshape changes associated with spectral diffusion. We expect $\nu_{SE}(t_2)$ extracted from ν_1 slices taken near the center of the peak to have smaller contributions associated with spectral diffusion for systems with larger Stokes shifts. To further investigate this, we expand upon the Kubo lineshape model and simulate 2DES spectra using the displaced oscillator model where the relaxation of the S_1 state is included.[74,98] The simulated spectra and extracted $\nu_{SE}(t_2)$ are plotted in Figure S16 of the Supporting Information. Comparison of the early and late time values of $\nu_{SE}(t_2)$ from the simulated spectra show that slices taken from the center of the peak are better able to reproduce the Stokes shift, further supporting that spectral diffusion lineshape changes will have a minimal contribution to the extracted $\nu_{SE}(t_2)$ for slices obtained near the center of the peak. As an additional test, we have also performed a global analysis of slices taken at different ν_1 frequencies (see Supporting Information, section 6). From the global analysis we find that spectral features associated with the growth of the stimulated emission are more pronounced for slices taken toward the center of the peak when compared to slices taken on the red or blue edge.

Considering how the spectral changes associated with spectral diffusion and vibrational relaxation contribute to ν_{SE}, the comparison of the extracted timescales indicates that contributions from these different processes will be minimized in the analysis of $S(t)$ for ν_1 slices taken near the center of the peak in the 2DES spectra. In the context of the τ_{gau} timescales presented in Figure 6, this indicates that the fastest timescale components at the center of the peak as reporting on the ultrafast solvation dynamics, where the longer timescales on the red and blue edges are attributed to a combination of contributions arising from the solvent reorganization, vibrational relaxation, and spectral diffusion. As such, taking slices along the ν_1 axis of the 2DES spectra can serve as a means for disentangling the contribution of the solvation dynamics from ultrafast vibrational relaxation.

CONCLUSIONS

In this work, we extract the frequency-dependent dynamic Stokes shift function from 2DES spectra that exhibit strong oscillatory components associated with vibrational coherences. To accomplish this we expanded on a general procedure to extract $S(t)$ from 2D electronic spectra[50] to include oscillatory components associated with the evolution of vibrational coherences. Though previous studies have considered this through a global analysis of the entire 2D electronic spectra simultaneously spanning the ν_1,ν_3 coordinates,[49] the advantage of the current procedure lies in its ability to be applied to a single slice along the excitation axis, enabling for the excitation frequency dependence of the solvation dynamics to be

https://dx.doi.org/10.1021/acs.jpcb.0c05522
J. Phys. Chem. B 2020, 124, 8857−8867

investigated. Applying the analysis procedure to slices taken at different excitation frequencies, we obtain the ultrafast timescales associated with $S(t)$ as a function of excitation frequency. Through comparison, we find that the fastest timescales of ~36 fs are extracted over a certain excitation frequency window where contributions from lineshape changes associated with spectral diffusion and vibrational relaxation are minimized. The fastest τ_{gau} timescales extracted are attributed to the solvent inertial response. The longer τ_{gau} timescales on the red and blue edges of the peak are attributed to contributions arising from lineshape changes associated with vibrational relaxation and spectral diffusion in the 2DES spectra. In this sense, examining the ν_1 frequency dependence of the solvation dynamics could serve as a means for separating intramolecular vibrational relaxation timescales from the inertial solvent response.

■ ASSOCIATED CONTENT

Supporting Information

The Supporting Information is available free of charge at https://pubs.acs.org/doi/10.1021/acs.jpcb.0c05522.

A detailed description of the laser pulse characterization, DFT and TD-DFT calculations, procedures of extracting the dynamic Stokes shift and ultrafast timescales, experimental results for 2DES obtained under different pulse tuning conditions, model 2DES spectra for interpreting the ν_1 frequency dependence of spectral diffusion, and a comparison of the dynamic Stokes shift and a global analysis (PDF)

■ AUTHOR INFORMATION

Corresponding Author

Jessica M. Anna − *University of Pennsylvania, Philadelphia, Pennsylvania 19104, United States;* orcid.org/0000-0001-5440-6987; Email: jmanna@sas.upenn.edu

Authors

Jiawei Lu − *University of Pennsylvania, Philadelphia, Pennsylvania 19104, United States*

Yumin Lee − *University of Pennsylvania, Philadelphia, Pennsylvania 19104, United States;* orcid.org/0000-0003-4905-4870

Complete contact information is available at: https://pubs.acs.org/10.1021/acs.jpcb.0c05522

Notes

The authors declare no competing financial interest.

■ ACKNOWLEDGMENTS

The authors acknowledge support for this work by the U.S. Department of Energy, Office of Science, Office of Basic Energy Sciences under award number DE-SC-0016043, the Center for Sustainable Separations of Metals (CSSM), a National Science Foundation Center for Chemical Innovation under award number CHE-1925708, and the Alfred P. Sloan Fellowship. Graduate student J.L. was supported by the CSSM (CHE-1925708) and the Vagelos Institute of Energy Science and Technology Graduate Fellowship. Graduate student Y.L. was supported by the DOE DE-SC-0016043 award.

■ REFERENCES

(1) Bagchi, B.; Jana, B. Solvation Dynamics in Dipolar Liquids. *Chem. Soc. Rev.* **2010**, *39*, 1936−1954.

(2) Rosspeintner, A.; Lang, B.; Vauthey, E. Ultrafast Photochemistry in Liquids. *Annu. Rev. Phys. Chem.* **2013**, *64*, 247−271.

(3) Kumpulainen, T.; Lang, B.; Rosspeintner, A.; Vauthey, E. Ultrafast Elementary Photochemical Processes of Organic Molecules in Liquid Solution. *Chem. Rev.* **2017**, *117*, 10826−10939.

(4) Stratt, R. M.; Maroncelli, M. Nonreactive Dynamics in Solution: The Emerging Molecular View of Solvation Dynamics and Vibrational Relaxation. *J. Phys. Chem.* **1996**, *100*, 12981−12996.

(5) Maroncelli, M. The Dynamics of Solvation in Polar Liquids. *J. Mol. Liq.* **1993**, *57*, 1−37.

(6) Fleming, G. R.; Cho, M. Chromophore-Solvent Dynamics. *Annu. Rev. Phys. Chem.* **1996**, *47*, 109−134.

(7) Horng, M. L.; Gardecki, J. A.; Papazyan, A.; Maroncelli, M. Subpicosecond Measurements of Polar Solvation Dynamics: Coumarin 153 Revisited. *J. Phys. Chem.* **1995**, *99*, 17311−17337.

(8) Joo, T.; Jia, Y.; Yu, J. Y.; Lang, M. J.; Fleming, G. R. Third-Order Nonlinear Time Domain Probes of Solvation Dynamics. *J. Chem. Phys.* **1996**, *104*, 6089−6108.

(9) Kumar, P. V.; Maroncelli, M. Polar Solvation Dynamics of Polyatomic Solutes: Simulation Studies in Acetonitrile and Methanol. *J. Chem. Phys.* **1995**, *103*, 3038−3060.

(10) Rosenthal, S. J.; Xie, X.; Du, M.; Fleming, G. R. Femtosecond Solvation Dynamics in Acetonitrile: Observation of the Inertial Contribution to the Solvent Response. *J. Chem. Phys.* **1991**, *95*, 4715−4718.

(11) Fonseca, T.; Ladanyi, B. M. Breakdown of Linear Response for Solvation Dynamics in Methanol. *J. Phys. Chem.* **1991**, *95*, 2116−2119.

(12) Rosenthal, S. J.; Jimenez, R.; Fleming, G. R.; Kumar, P. V.; Maroncelli, M. Solvation Dynamics in Methanol: Experimental and Molecular Dynamics Simulation Studies. *J. Mol. Liq.* **1994**, *60*, 25−56.

(13) Bagchi, B. Dynamics Of Solvation And Charge Transfer Reactions In Dipolar Liquids. *Annu. Rev. Phys. Chem.* **1989**, *40*, 115−141.

(14) Nandi, N.; Roy, S.; Bagchi, B. Ultrafast Solvation Dynamics in Water: Isotope Effects and Comparison with Experimental Results. *J. Chem. Phys.* **1995**, *102*, 1390−1397.

(15) McHale, J. L. Subpicosecond Solvent Dynamics in Charge-Transfer Transitions: Challenges and Opportunities in Resonance Raman Spectroscopy. *Acc. Chem. Res.* **2001**, *34*, 265−272.

(16) Carter, E. A.; Hynes, J. T. Solvation Dynamics for an Ion Pair in a Polar Solvent: Time-Dependent Fluorescence and Photochemical Charge Transfer. *J. Chem. Phys.* **1991**, *94*, 5961−5979.

(17) Feskov, S. V.; Mikhailova, V. A.; Ivanov, A. I. Non-Equilibrium Effects in Ultrafast Photoinduced Charge Transfer Kinetics. *J. Photochem. Photobiol. C Photochem. Rev.* **2016**, *29*, 48−72.

(18) Dereka, B.; Vauthey, E. Solute-Solvent Interactions and Excited-State Symmetry Breaking: Beyond the Dipole-Dipole and the Hydrogen-Bond Interactions. *J. Phys. Chem. Lett.* **2017**, *8*, 3927−3932.

(19) Delor, M.; Sazanovich, I. V.; Towrie, M.; Weinstein, J. A. Probing and Exploiting the Interplay between Nuclear and Electronic Motion in Charge Transfer Processes. *Acc. Chem. Res.* **2015**, *48*, 1131−1139.

(20) Hammes-Schiffer, S.; Soudackov, A. V. Proton-Coupled Electron Transfer in Solution, Proteins, and Electrochemistry. *J. Phys. Chem. B* **2008**, *112*, 14108−14123.

(21) Walker, G. C.; Aakesson, E.; Johnson, A. E.; Levinger, N. E.; Barbara, P. F. Interplay of Solvent Motion and Vibrational Excitation in Electron-Transfer Kinetics: Experiment and Theory. *J. Phys. Chem.* **1992**, *96*, 3728−3736.

(22) Nazarov, A. E.; Barykov, V. Y.; Ivanov, A. I. Effect of Intramolecular High-Frequency Vibrational Mode Excitation on Ultrafast Photoinduced Charge Transfer and Charge Recombination Kinetics. *J. Phys. Chem. B* **2016**, *120*, 3196−3205.

(23) Huang, Y.; Rettner, C. T.; Auerbach, D. J.; Wodtke, A. M. Vibrational Promotion of Electron Transfer. *Science* **2000**, *290*, 111−114.
(24) Cho, M. Coherent Two-Dimensional Optical Spectroscopy. *Chem. Rev.* **2008**, *108*, 1331−1418.
(25) Nuernberger, P.; Ruetzel, S.; Brixner, T. Multidimensional Electronic Spectroscopy of Photochemical Reactions. *Angew. Chem., Int. Ed.* **2015**, *54*, 11368−11386.
(26) Ogilvie, J. P.; Kubarych, K. J. Chapter 5 Multidimensional Electronic and Vibrational Spectroscopy. In *Advances in Atomic, Molecular and Optical Physics*; 2009; Vol. *57*, pp. 249−321.
(27) Anna, J. M.; Song, Y.; Dinshaw, R.; Scholes, G. D. Two-Dimensional Electronic Spectroscopy for Mapping Molecular Photophysics. *Pure Appl. Chem.* **2013**, *85*, 1307−1319.
(28) Jonas, D. M. Vibrational and Nonadiabatic Coherence in 2D Electronic Spectroscopy, the Jahn−Teller Effect, and Energy Transfer. *Annu. Rev. Phys. Chem.* **2018**, *69*, 327−352.
(29) Dostál, J.; Benešová, B.; Brixner, T. Two-Dimensional Electronic Spectroscopy Can Fully Characterize the Population Transfer in Molecular Systems. *J. Chem. Phys.* **2016**, *145*, 124312.
(30) Jonas, D. M. Two-Dimensional Femtosecond Spectroscopy. *Annu. Rev. Phys. Chem.* **2003**, *54*, 425−463.
(31) Hybl, J. D.; Albrecht, A. W.; Gallagher Faeder, S. M.; Jonas, D. M. Two-Dimensional Electronic Spectroscopy. *Chem. Phys. Lett.* **1998**, *297*, 307−313.
(32) Faeder, S. M. G.; Jonas, D. M. Two-Dimensional Electronic Correlation and Relaxation Spectra: Theory and Model Calculations. *J. Phys. Chem. A* **1999**, *103*, 10489−10505.
(33) Jonas, D. M.; Bradforth, S. E.; Passino, S. A.; Fleming, G. R. Femtosecond Wavepacket Spectroscopy: Influence of Temperature, Wavelength, and Pulse Duration. *J. Phys. Chem.* **1995**, *99*, 2594−2608.
(34) Heller, E. J. The Semiclassical Way to Molecular Spectroscopy. *Acc. Chem. Res.* **1981**, *14*, 368−375.
(35) Pollard, W. T.; Dexheimer, S. L.; Wang, Q.; Peteanu, L. A.; Shank, C. V.; Mathies, R. A. Theory of Dynamic Absorption Spectroscopy of Nonstationary States. 4. Application to 12-Fs Resonant Impulsive Raman Spectroscopy of Bacteriorhodopsin. *J. Phys. Chem.* **1992**, *96*, 6147−6158.
(36) Pollard, W. T.; Lee, S. Y.; Mathies, R. A. Wave Packet Theory of Dynamic Absorption Spectra in Femtosecond Pump-Probe Experiments. *J. Chem. Phys.* **1990**, *92*, 4012−4029.
(37) Nemeth, A.; Milota, F.; Mančal, T.; Lukeš, V.; Kauffmann, H. F.; Sperling, J. Vibronic Modulation of Lineshapes in Two-Dimensional Electronic Spectra. *Chem. Phys. Lett.* **2008**, *459*, 94−99.
(38) Egorova, D.; Gelin, M. F.; Domcke, W. Analysis of Cross Peaks in Two-Dimensional Electronic Photon-Echo Spectroscopy for Simple Models with Vibrations and Dissipation. *J. Chem. Phys.* **2007**, *126*, No. 074314.
(39) Egorova, D. Oscillations in Two-Dimensional Photon-Echo Signals of Excitonic and Vibronic Systems: Stick-Spectrum Analysis and Its Computational Verification. *J. Chem. Phys.* **2014**, *140*, No. 034314.
(40) Nemeth, A.; Milota, F.; Mančal, T.; Lukeš, V.; Hauer, J.; Kauffmann, H. F.; Sperling, J. Vibrational Wave Packet Induced Oscillations in Two-Dimensional Electronic Spectra. I. Experiments. *J. Chem. Phys.* **2010**, *132*, 184514.
(41) Mančal, T.; Nemeth, A.; Milota, F.; Lukeš, V.; Kauffmann, H. F.; Sperling, J. Vibrational Wave Packet Induced Oscillations in Two-Dimensional Electronic Spectra. II. Theory. *J. Chem. Phys.* **2010**, *132*, 184515.
(42) Tekavec, P. F.; Myers, J. A.; Lewis, K. L. M.; Ogilvie, J. P. Two-Dimensional Electronic Spectroscopy with a Continuum Probe. *Opt. Lett.* **2009**, *34*, 1390−1392.
(43) Caram, J. R.; Fidler, A. F.; Engel, G. S. Excited and Ground State Vibrational Dynamics Revealed by Two-Dimensional Electronic Spectroscopy. *J. Chem. Phys.* **2012**, *137*, No. 024507.
(44) Dean, J. C.; Rafiq, S.; Oblinsky, D. G.; Cassette, E.; Jumper, C. C.; Scholes, G. D. Broadband Transient Absorption and Two-Dimensional Electronic Spectroscopy of Methylene Blue. *J. Phys. Chem. A* **2015**, *119*, 9098−9108.
(45) Egorova, D.; Gelin, M. F.; Domcke, W. Analysis of Vibrational Coherences in Homodyne and Two-Dimensional Heterodyne Photon-Echo Spectra of Nile Blue. *Chem. Phys.* **2007**, *341*, 113−122.
(46) Fransted, K. A.; Engel, G. S. Probing Vibrational Dynamics of PM650 with Two-Dimensional Electronic Spectroscopy. *Chem. Phys.* **2012**, *403*, 59−67.
(47) Hybl, J. D.; Christophe, Y.; Jonas, D. M. Peak Shapes in Femtosecond 2D Correlation Spectroscopy. *Chem. Phys.* **2001**, *266*, 295−309.
(48) Hybl, J. D.; Yu, A.; Farrow, D. A.; Jonas, D. M. Polar Solvation Dynamics in the Femtosecond Evolution of Two-Dimensional Fourier Transform Spectra. *J. Phys. Chem. A* **2002**, *106*, 7651−7654.
(49) Bolzonello, L.; Polo, A.; Volpato, A.; Meneghin, E.; Cordaro, M.; Trapani, M.; Fortino, M.; Pedone, A.; Castriciano, M. A.; Collini, E. Two-Dimensional Electronic Spectroscopy Reveals Dynamics and Mechanisms of Solvent-Driven Inertial Relaxation in Polar BODIPY Dyes. *J. Phys. Chem. Lett.* **2018**, *9*, 1079−1085.
(50) Lee, Y.; Das, S.; Malamakal, R. M.; Meloni, S.; Chenoweth, D. M.; Anna, J. M. Ultrafast Solvation Dynamics and Vibrational Coherences of Halogenated Boron-Dipyrromethene Derivatives Revealed through Two-Dimensional Electronic Spectroscopy. *J. Am. Chem. Soc.* **2017**, *139*, 14733−14742.
(51) Myers, J. A.; Lewis, K. L.; Tekavec, P. F.; Ogilvie, J. P. Two-Color Two-Dimensional Fourier Transform Electronic Spectroscopy with a Pulse-Shaper. *Opt. Express* **2008**, *16*, 17420−17428.
(52) Nitzan, A. *Chemical Dynamics in Condensed Phases: Relaxation, Transfer, And Reactions In Condensed Molecular Systems*; Oxford University Press: New York, 2006.
(53) Roberts, S. T.; Loparo, J. J.; Tokmakoff, A. Characterization of Spectral Diffusion from Two-Dimensional Line Shapes. *J. Chem. Phys.* **2006**, *125*, No. 084502.
(54) Wells, K. L.; Zhang, Z.; Rouxel, J. R.; Tan, H. S. Measuring the Spectral Diffusion of Chlorophyll a Using Two-Dimensional Electronic Spectroscopy. *J. Phys. Chem. B* **2013**, *117*, 2294−2299.
(55) Šanda, F.; Perlík, V.; Lincoln, C. N.; Hauer, J. Center Line Slope Analysis in Two-Dimensional Electronic Spectroscopy. *J. Phys. Chem. A* **2015**, *119*, 10893−10909.
(56) Moca, R.; Meech, S. R.; Heisler, I. A. Two-Dimensional Electronic Spectroscopy of Chlorophyll a: Solvent Dependent Spectral Evolution. *J. Phys. Chem. B* **2015**, *119*, 8623−8630.
(57) Lazonder, K.; Pshenichnikov, M. S.; Wiersma, D. A. Easy Interpretation of Optical Two-Dimensional Correlation Spectra. *Opt. Lett.* **2006**, *31*, 3354−3356.
(58) Hybl, J. D.; Faeder, S. M. G.; Albrecht, A. W.; Tolbert, C. A.; Green, D. C.; Jonas, D. M. Time and Frequency Resolved Femtosecond Solvent Dynamics. *J. Lumin.* **2000**, *87-89*, 126−129.
(59) Turner, D. B.; Wilk, K. E.; Curmi, P. M. G.; Scholes, G. D. Comparison of Electronic and Vibrational Coherence Measured by Two-Dimensional Electronic Spectroscopy. *J. Phys. Chem. Lett.* **2011**, *2*, 1904−1911.
(60) Heisler, I. A.; Moca, R.; Camargo, F. V. A.; Meech, S. R. Two-Dimensional Electronic Spectroscopy Based on Conventional Optics and Fast Dual Chopper Data Acquisition. *Rev. Sci. Instrum.* **2014**, *85*, No. 063103.
(61) Spokoyny, B.; Koh, C. J.; Harel, E. Stable and High-Power Few Cycle Supercontinuum for 2D Ultrabroadband Electronic Spectroscopy. *Opt. Lett.* **2015**, *40*, 1014−1017.
(62) Bizimana, L. A.; Brazard, J.; Carbery, W. P.; Gellen, T.; Turner, D. B. Resolving Molecular Vibronic Structure Using High-Sensitivity Two-Dimensional Electronic Spectroscopy. *J. Chem. Phys.* **2015**, *143*, 164203.
(63) Roeding, S.; Klimovich, N.; Brixner, T. Optimizing Sparse Sampling for 2D Electronic Spectroscopy. *J. Chem. Phys.* **2017**, *146*, 84201.
(64) Carbery, W. P.; Pinto-Pacheco, B.; Buccella, D.; Turner, D. B. Resolving the Fluorescence Quenching Mechanism of an Oxazine

https://dx.doi.org/10.1021/acs.jpcb.0c05522
J. Phys. Chem. B 2020, 124, 8857−8867

Dye Using Ultrabroadband Two-Dimensional Electronic Spectroscopy. *J. Phys. Chem. A* **2019**, *123*, 5072−5080.
(65) Rafiq, S.; Scholes, G. D. Slow Intramolecular Vibrational Relaxation Leads to Long-Lived Excited-State Wavepackets. *J. Phys. Chem. A* **2016**, *120*, 6792−6799.
(66) Brazard, J.; Bizimana, L. A.; Gellen, T.; Carbery, W. P.; Turner, D. B. Experimental Detection of Branching at a Conical Intersection in a Highly Fluorescent Molecule. *J. Phys. Chem. Lett.* **2016**, *7*, 14−19.
(67) Brazard, J.; Bizimana, L. A.; Turner, D. B. Accurate Convergence of Transient-Absorption Spectra Using Pulsed Lasers. *Rev. Sci. Instrum.* **2015**, *86*, 53106.
(68) Fuji, T.; Saito, T.; Kobayashi, T. Dynamical Observation of Duschinsky Rotation by Sub-5-Fs Real-Time Spectroscopy. *Chem. Phys. Lett.* **2000**, *332*, 324−330.
(69) Fujiyoshi, S.; Ishibashi, T.-a.; Onishi, H. Low-Frequency Vibrations of Molecular Submonolayers Detected by Time-Domain Raman Spectroscopy. *J. Mol. Struct.* **2005**, *735-736*, 169−177.
(70) Vogel, E.; Gbureck, A.; Kiefer, W. Vibrational Spectroscopic Studies on the Dyes Cresyl Violet and Coumarin 152. *J. Mol. Struct.* **2000**, *550-551*, 177−190.
(71) Cho, M. *Two-Dimensional Optical Spectroscopy*; CRC Press: Boca Raton, 2009.
(72) Hamm, P.; Zanni, M. *Concepts and Methods of 2D Infrared Spectroscopy*; Cambridge University Press: Cambridge, 2011.
(73) Mukamel, S. Multidimensional Femtosecond Correlation Spectroscopies of Electronic and Vibrational Excitations. *Annu. Rev. Phys. Chem.* **2000**, *51*, 691−729.
(74) Mukamel, S. *Principles of Nonlinear Optical Spectroscopy*; Oxford University Press: New York, 1999.
(75) Lee, Y.; Gorka, M.; Golbeck, J. H.; Anna, J. M. Ultrafast Energy Transfer Involving the Red Chlorophylls of Cyanobacterial Photosystem I Probed through Two-Dimensional Electronic Spectroscopy. *J. Am. Chem. Soc.* **2018**, *140*, 11631−11638.
(76) Shim, S.-H.; Zanni, M. T. How to Turn Your Pump−Probe Instrument into a Multidimensional Spectrometer: 2D IR and Vis Spectroscopiesvia Pulse Shaping. *Phys. Chem. Chem. Phys.* **2009**, *11*, 748−761.
(77) Grumstrup, E. M.; Shim, S.-H.; Montgomery, M. A.; Damrauer, N. H.; Zanni, M. T. Facile Collection of Two-Dimensional Electronic Spectra Using Femtosecond Pulse-Shaping Technology. *Opt. Express* **2007**, *15*, 16681−16889.
(78) DeFlores, L. P.; Nicodemus, R. A.; Tokmakoff, A. Two-Dimensional Fourier Transform Spectroscopy in the Pump-Probe Geometry. *Opt. Lett.* **2007**, *32*, 2966−2968.
(79) DeLong, K. W.; Trebino, R.; Hunter, J.; White, W. E. Frequency-Resolved Optical Gating with the Use of Second-Harmonic Generation. *J. Opt. Soc. Am. B* **1994**, *11*, 2206−2215.
(80) Frisch, G. W.; Schlegel, H. B.; Scuseria, G. E.; Robb, M. A.; Cheeseman, J. R.; Scalmani, G.; Barone, V.; Petersson, G. A.; Nakatsuji, H.; Li, X.; et al. *Gaussian 16*, Rev. A.03. Gaussian, Inc.: Wallingford, CT, 2016.
(81) Jacquemin, D.; Planchat, A.; Adamo, C.; Mennucci, B. TD-DFT Assessment of Functionals for Optical 0-0 Transitions in Solvated Dyes. *J. Chem. Theory Comput.* **2012**, *8*, 2359−2372.
(82) Jimenez, R.; Fleming, G. R.; Kumar, P. V.; Maroncelli, M. Femtosecond Solvation Dynamics of Water. *Nature* **1994**, *369*, 471−473.
(83) Jumper, C. C.; Arpin, P. C.; Turner, D. B.; McClure, S. D.; Rafiq, S.; Dean, J. C.; Cina, J. A.; Kovac, P. A.; Mirkovic, T.; Scholes, G. D. Broad-Band Pump−Probe Spectroscopy Quantifies Ultrafast Solvation Dynamics of Proteins and Molecules. *J. Phys. Chem. Lett.* **2016**, *7*, 4722−4731.
(84) Christensson, N.; Dietzek, B.; Yartsev, A.; Pullerits, T. Solute Specific Polar Solvation Studied by Photon Echo Spectroscopy. *Chem. Phys.* **2009**, *357*, 85−95.
(85) de Boeij, W. P.; Pshenichnikov, M. S.; Wiersma, D. A. Ultrafast Solvation Dynamics Explored by Femtosecond Photon Echo Spectroscopy. *Annu. Rev. Phys. Chem.* **1998**, *49*, 99−123.
(86) Ohta, K.; Larsen, D. S.; Yang, M.; Fleming, G. R. Influence of Intramolecular Vibrations in Third-Order, Time-Domain Resonant Spectroscopies. II. Numerical Calculations. *J. Chem. Phys.* **2001**, *114*, 8020−8039.
(87) Larsen, D. S.; Ohta, K.; Xu, Q. H.; Cyrier, M.; Fleming, G. R. Influence of Intramolecular Vibrations in Third-Order, Time-Domain Resonant Spectroscopies. I. Experiments. *J. Chem. Phys.* **2001**, *114*, 8008−8019.
(88) Eom, I.; Joo, T. Polar Solvation Dynamics of Coumarin 153 by Ultrafast Time-Resolved Fluorescence. *J. Chem. Phys.* **2009**, *131*, 244507.
(89) van Stokkum, I. H. M.; Jumper, C. C.; Snellenburg, J. J.; Scholes, G. D.; van Grondelle, R.; Malý, P. Estimation of Damped Oscillation Associated Spectra from Ultrafast Transient Absorption Spectra. *J. Chem. Phys.* **2016**, *145*, 174201.
(90) Schott, S.; Ress, L.; Hrušák, J.; Nuernberger, P.; Brixner, T. Identification of Photofragmentation Patterns in Trihalide Anions by Global Analysis of Vibrational Wavepacket Dynamics in Broadband Transient Absorption Data. *Phys. Chem. Chem. Phys.* **2016**, *18*, 33287−33302.
(91) Sajadi, M.; Weinberger, M.; Wagenknecht, H. A.; Ernsting, N. P. Polar Solvation Dynamics in Water and Methanol: Search for Molecularity. *Phys. Chem. Chem. Phys.* **2011**, *13*, 17768−17774.
(92) Egorova, D. Self-Analysis of Coherent Oscillations in Time-Resolved Optical Signals. *J. Phys. Chem. A* **2014**, *118*, 10259−10267.
(93) Butkus, V.; Zigmantas, D.; Valkunas, L.; Abramavicius, D. Vibrational vs. Electronic Coherences in 2D Spectrum of Molecular Systems. *Chem. Phys. Lett.* **2012**, *545*, 40−43.
(94) Turner, D. B.; Dinshaw, R.; Lee, K. K.; Belsley, M. S.; Wilk, K. E.; Curmi, P. M. G.; Scholes, G. D. Quantitative Investigations of Quantum Coherence for a Light-Harvesting Protein at Conditions Simulating Photosynthesis. *Phys. Chem. Chem. Phys.* **2012**, *14*, 4857−4874.
(95) Kwac, K.; Cho, M. Molecular Dynamics Simulation Study of N-Methylacetamide in Water. II. Two-Dimensional Infrared Pump−Probe Spectra. *J. Chem. Phys.* **2003**, *119*, 2256−2263.
(96) Kwak, K.; Park, S.; Finkelstein, I. J.; Fayer, M. D. Frequency-Frequency Correlation Functions and Apodization in Two-Dimensional Infrared Vibrational Echo Spectroscopy: A New Approach. *J. Chem. Phys.* **2007**, *127*, 124503.
(97) Asbury, J. B.; Steinel, T.; Stromberg, C.; Corcelli, S. A.; Lawrence, C. P.; Skinner, J. L.; Fayer, M. D. Water Dynamics: Vibrational Echo Correlation Spectroscopy and Comparison to Molecular Dynamics Simulations. *J. Phys. Chem. A* **2004**, *108*, 1107−1119.
(98) Gu, Y.; Widom, A.; Champion, P. M. Spectral Line Shapes of Damped Quantum Oscillators: Applications to Biomolecules. *J. Chem. Phys.* **1994**, *100*, 2547−2560.

https://dx.doi.org/10.1021/acs.jpcb.0c05522
J. Phys. Chem. B 2020, 124, 8857−8867